Electronic Supporting Information (ESI) for

Ni-Co Hexacyanoferrate Hollow Nanoprism with CN vacancy for Electrocatalytic Benzyl Alcohol Oxidation

Chenghang Lv,[a, b] Liang Chen,[*a] Jingjing Bai,[a] Hongyu Ruo,[a] Yanlong Pan,[a] Shoudong Xu,[c] Jiaqi Chen,[a] Ding Zhang,[d] and Chunli Guo,[*b]

[a] College of Chemistry, Taiyuan University of Technology, Taiyuan 030024, P. R. China. Email: chenliang@tyut.edu.cn

[b] College of Materials Science and Engineering, Taiyuan University of Technology, Taiyuan 030024, P. R. China. Email: guochunli@tyut.edu.cn

[c] College of Chemical Engineering and Technology, Taiyuan University of Technology, Taiyuan 030024, P. R. China.

[d] School of Chemical Engineering and Pharmacy, Wuhan Institute of Technology, Wuhan 430205, P. R. China.

Experimental Section

Materials and Chemicals.

Nickel acetate tetrahydrate [$Ni(CH_3COO)_2 \cdot 4H_2O$], cobalt acetate tetrahydrate [$Co(CH_3COO)_2 \cdot 4H_2O$], benzyl alcohol, benzaldehyde, benzoic acid, and ethyl acetate were obtained from Aladdin Reagent Co., Ltd. $K_3[Fe(CN)_6]$, polyvinylpyrrolidone (PVP K-30, MW ~10000), and KOH were purchased from Sinopharm Chemical Reagent Co., Ltd. Ethanol and hydrochloric acid (HCl) were purchased from Xilong Chemical Reagent Co. Ltd. Carbon paper was obtained from Changde Liyuan New Material Co. Ltd. All reagents were of analytical grade and used as received without further purification.

Synthesis of precursors of Ni_xCo_1 nanoprisms.

The synthesis for Ni_xCo_1 nanoprisms precursors with varying Ni/Co ratios was conducted with slightly modifications based on a previous report [S1]. In a typical synthesis, 4.0 g of PVP K-30 and 1.5 g of a mixture of metal acetate tetrahydrate with different molar ratios of Ni/Co (1:0, 3:1, 2:1, or 1:1) were dissolved into 200 mL of ethanol at room temperature, forming a clear solution. The solution was then heated to 80 ℃ under refluxing conditions. After a 4-hour reaction, the resulting precipitate was collected via centrifugation, thoroughly rinsed with ethanol to remove attached PVP on the surface, and subsequently dried in air at 60 ℃. The

obtained products were labeled as Ni-pre, Ni_3Co_1-pre, Ni_2Co_1-pre, and Ni_1Co_1-pre.

Synthesis of Ni_xCo_1 hexacyanoferrate hollow nanoprisms.

The Ni_xCo_1 hollow nanoprisms (Ni_xCo_1-HCF HN) were through a straightforward solution synthesis method. In a typical synthesis of Ni_2Co_1Fe-HCF HN, 50 mg of Ni_2Co_1-pre was redispersed into 100 mL of ethanol using ultrasonic treatment, and 50 mg of $K_3[Fe(CN)_6]$ was dissolved in 100 mL of deionized water. Then, the $K_3[Fe(CN)_6]$ solution was added to the precursor dispersion under magnetic stirring. After stirring for 10 min at room temperature, the product was collected by centrifugation, washed with water and ethanol several times, and dried at 70°C overnight. The obtained products were labeled as Ni-HCF HN, Ni_3Co_1-HCF HN, Ni_2Co_1-HCF HN, and Ni_1Co_1-HCF HN.

Material characterization.

Powder X-ray diffraction (XRD) analysis was performed using a Bruker D8 Advance powder diffractometer equipped with Cu Kα X-ray radiation (λ = 1.5406 Å). Scanning electron microscopy (SEM) images were acquired by FEI Talos-S. High-angle annular dark field scanning transmission electron microscopy (HAADF-STEM) images were captured on a FEI Titan Themis Z microscope equipped with a probe-forming aberration corrector, operating at 300 kV. X-ray photoelectron spectroscopy (XPS) spectra were collected using a Thermo ESCALAB

250Xi X-ray photoelectron spectrometer. The shift of the binding energy was corrected using C 1s as an internal standard at 284.8 eV. Raman spectra were obtained with a Renishaw micro-Raman spectrometer via a laser (532 nm) as the exciting source. ESR spectra were obtained from a Bruker EMX PLUS.

Electrochemical measurements.

Electrochemical measurements were conducted using a Corrtest CS3104 electrochemical workstation with a three-electrode system, in which graphite rod and Hg/HgO electrode were selected as the counter electrode and reference electrode, respectively. The catalyst ink was prepared by dispersing 4.0 mg of the sample and 1.0 mg of carbon black in a mixture of 40 μL Nafion solution, 250 μL 2-propanol, and 750 μL water. After ultrasonication for 1 h, 4 μL of the prepared ink was drop-cast onto the polished glassy carbon electrode (disk area: 0.07065 cm^2) and dried in the air, leading to a final catalyst loading of 0.18 mg cm^2 . The applied potential was calibrated based on the reversible hydrogen electrode (RHE), using the equation of E (*vs*. RHE) = E (*vs*. Hg/HgO) + 0.098 V + 0.059 V × pH. The current density was normalized to the geometric area of the working electrode. The oxygen evolution reaction (OER) and benzyl alcohol oxidation reaction (BOR) experiments were performed in separate 30 mL solutions: 1 M KOH and 1 M KOH with 0.1 M benzyl alcohol, respectively. Prior to the electrochemical measurement, 20 cycles of cyclic

voltammetry (CV) were conducted at scan rate of 50 mV s^{-1} in the range of 0~0.6 V (*vs*. Hg/HgO) to stabilize the catalyst. To evaluate the performance of the catalysts, CV was performed at a scan rate of 5 mV s^{-1} in a potential window of 0~0.6 V (*vs*. Hg/HgO). The electrochemical surface area (ECSA) was determined through CV scans conducted within a potential range of 0.91~1.01 V (*vs*. RHE) with scanning rates ranged from 20 to 100 mV s^{-1}. The ECSA was calculated using the formula ECSA = C_{dl}/C_s, where C_{dl} and C_s correspond to the double layer capacitance and specific capacitance, respectively. The C_{dl} value can be evaluated by analyzing the slope between $\Delta j/2$ at 1.16 V (*vs*. RHE) and the scan rate. And C_s can be determined based on the scanning rate and the integral of $\frac{\int_{V_1}^{V_2} I\mathrm{d}V}{2\Delta V}$. Operando electrochemical impedance spectroscopy (EIS) was carried out at a potential range of 0 ~ 0.8 V (*vs*. Hg/HgO), with a frequency ranging from 0.1 Hz to 100 kHz and an amplitude of 5 mV.

Product analysis.

The products of BOR reaction were analyzed by gas chromatography (GC, Shanghai haixin GC-950) equipped with a flame ionization detector. Initially, the BOR was carried out at a constant potential of 1.44 V (*vs*. RHE). The resulting products were extracted with ethyl acetate and then analyzed by GC. 3 M HCl was added into the electrolyte after the BOR

reaction to achieve the conversion from Ph-COOK to Ph-COOH. Then, the Ph-COOH crystal containing KCl was separated by suction filtration from the electrolyte, and dried at 60 ℃ for 30 min.

The Coversion (%), yield (%) and reaction selectivity (%) of benzoic acid formation were calculated as follows:

$$\text{Coversion} = \frac{n(\text{reacted benzyl alcohol})}{n(\text{intial benzyl alcohol})} \times 100\%$$

$$\text{Selectivity} = \frac{n(\text{benzoic acid production})}{n(\text{reacted benzyl alcohol})} \times 100\%$$

$$\text{Yield} = \frac{n(\text{benzoic acid production})}{n(\text{intial benzyl alcohol})} \times 100\%$$

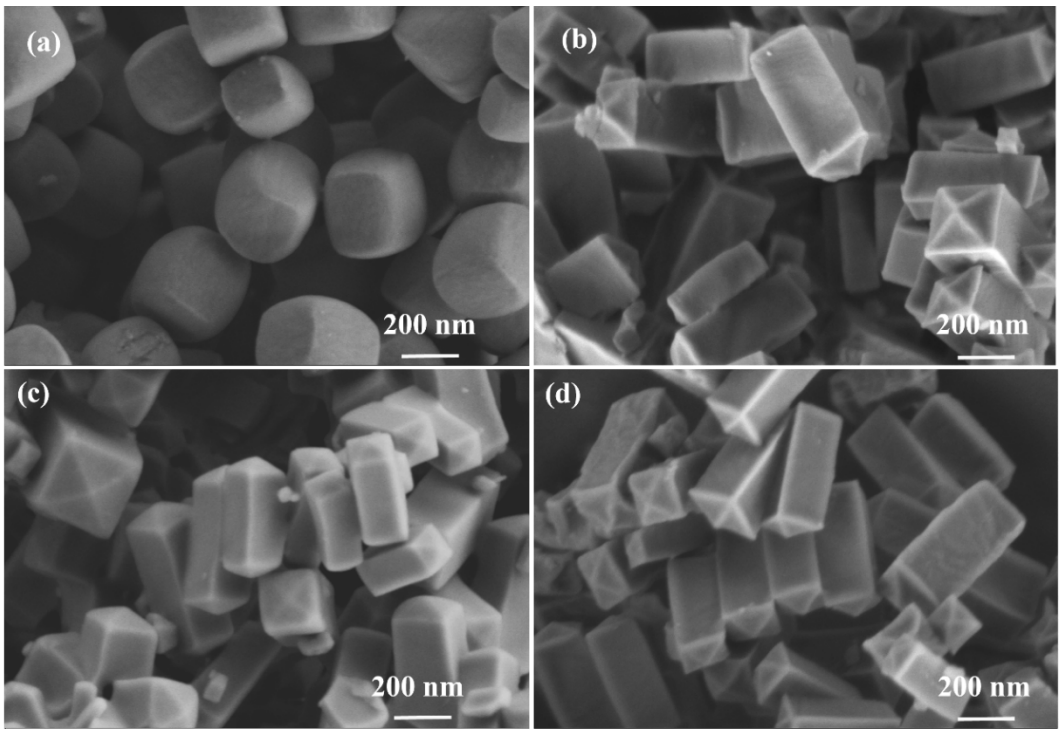

Fig. S1 SEM images of (a) Ni-pre, (b) Ni_3Co_1-pre, (c) Ni_2Co_1-pre, and (d) Ni_1Co_1-pre.

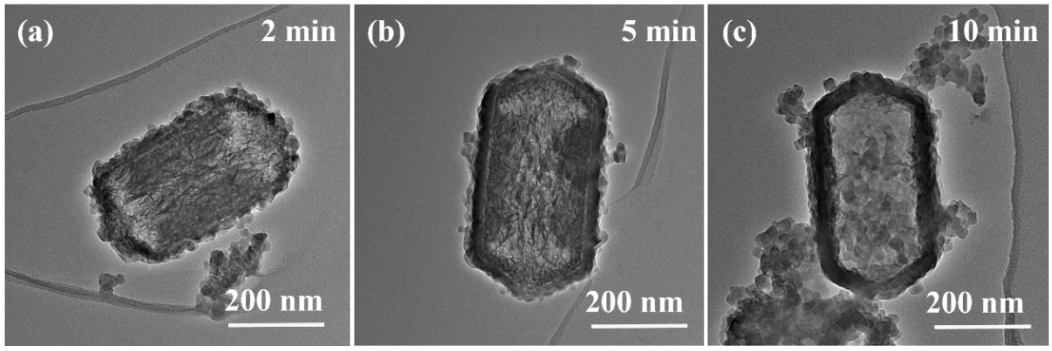

Fig. S2 TEM images of Ni_2Co_1-HCF HN with different reaction times. (a) 2 min, (b) 5 min, and (c) 10 min.

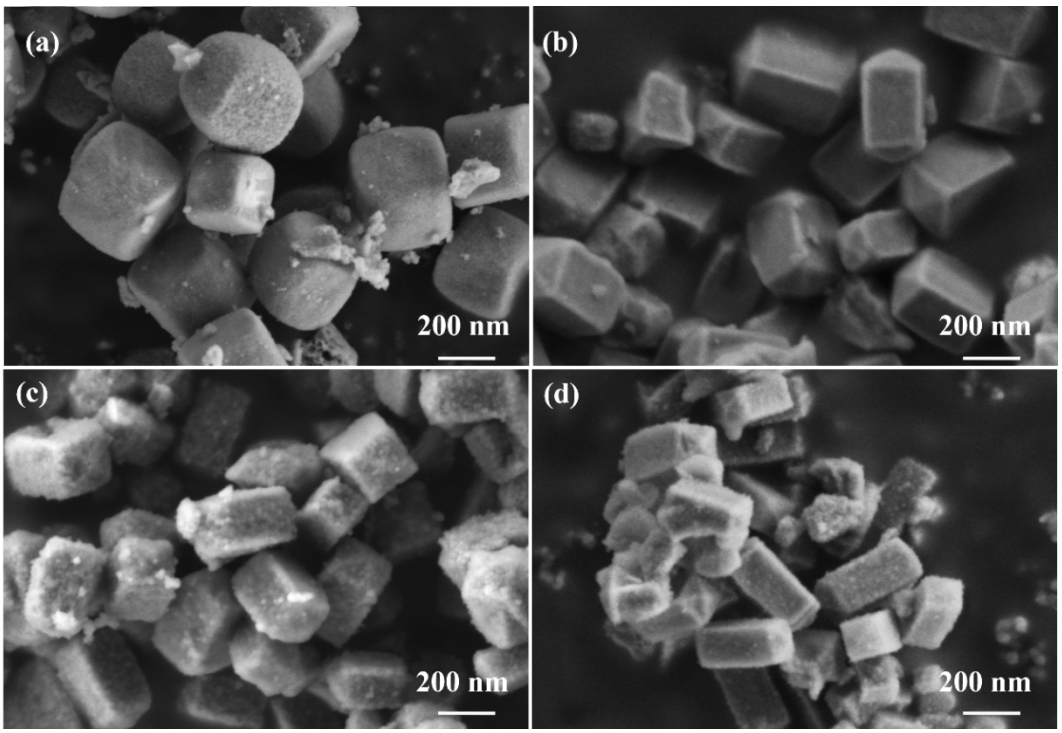

Fig. S3 SEM images of (a) Ni-HCF HN, (b) Ni_3Co_1-HCF HN, (c) Ni_xCo_1-HCF HN, and (d) Ni_1Co_1-HCF HN.

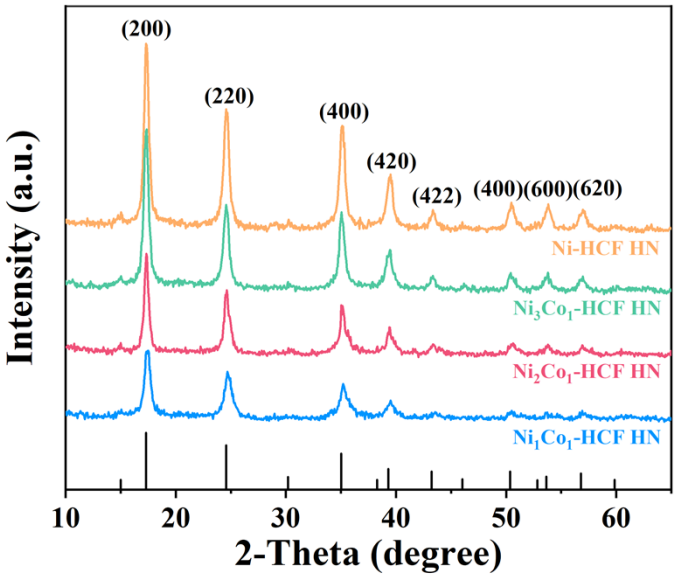

Fig. S4 XRD patterns of Ni_xCo_1-HCF HN.

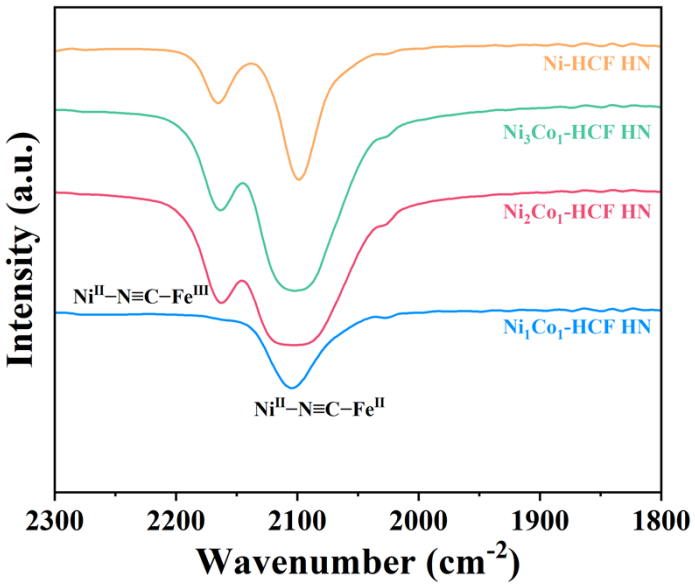

Fig. S5 FTIR spectroscopy of Ni_xCo_1-HCF HN.

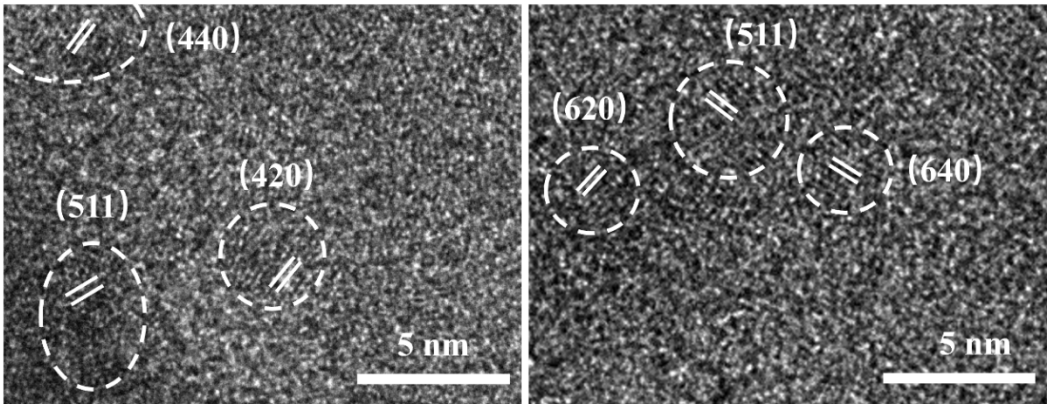

Fig. S6 HRTEM images of Ni_2Co_1-HCF HN

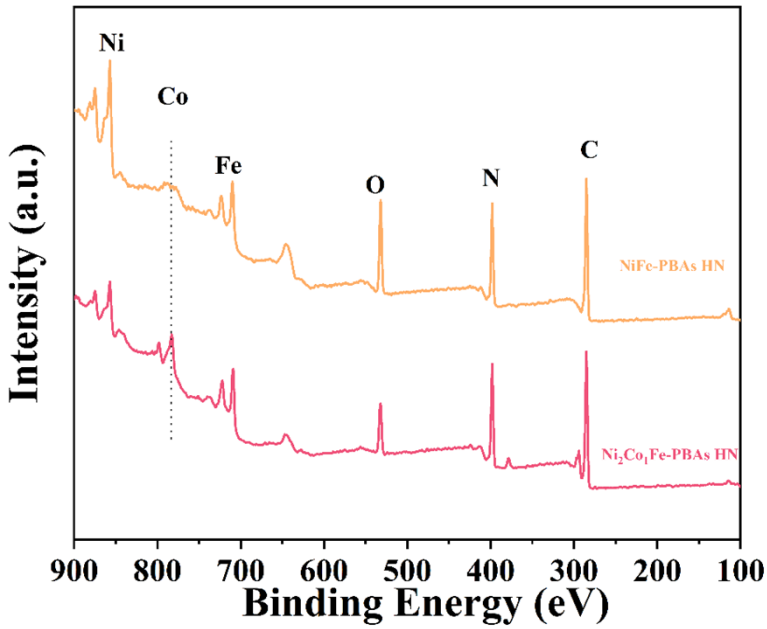

Fig. S7 XPS survey spectra of Ni-HCF and Ni_2Co_1-HCF HN

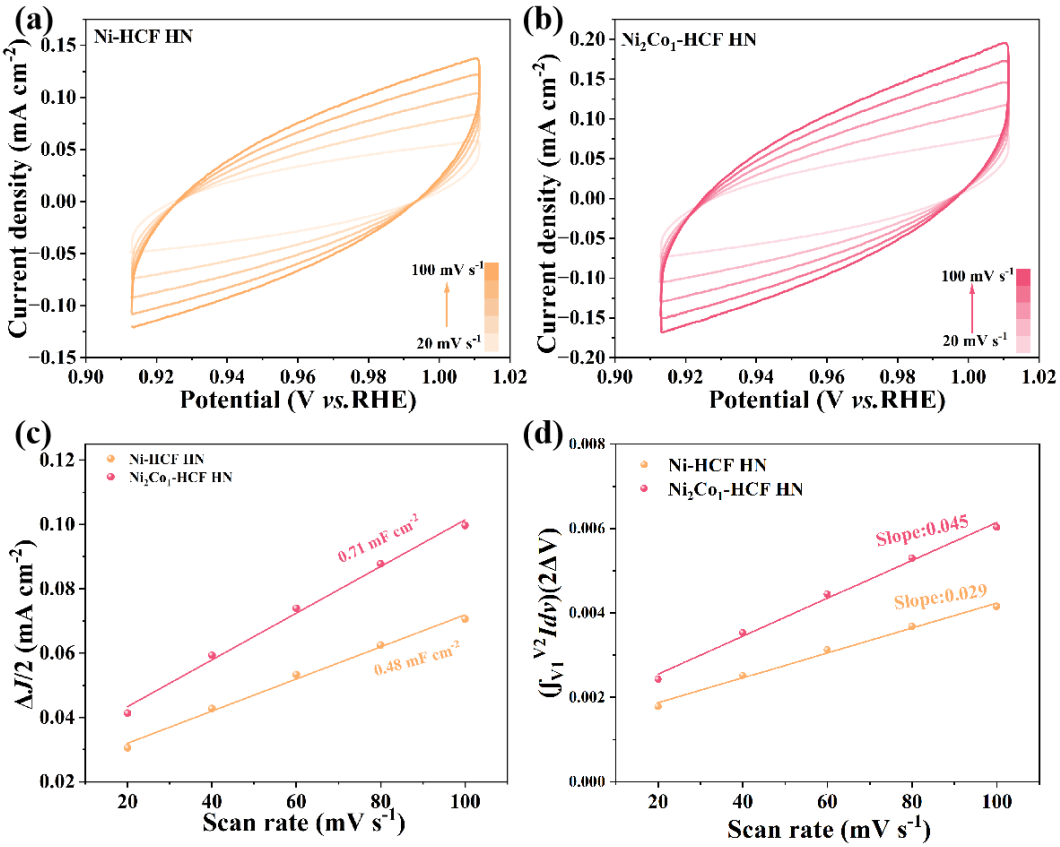

Fig. S8 CV curves of (a) Ni-HCF and (b) Ni_2Co_1-HCF HN in the non-Faraday region. (c) C_{dl} and (d) C_s for the corresponding samples.

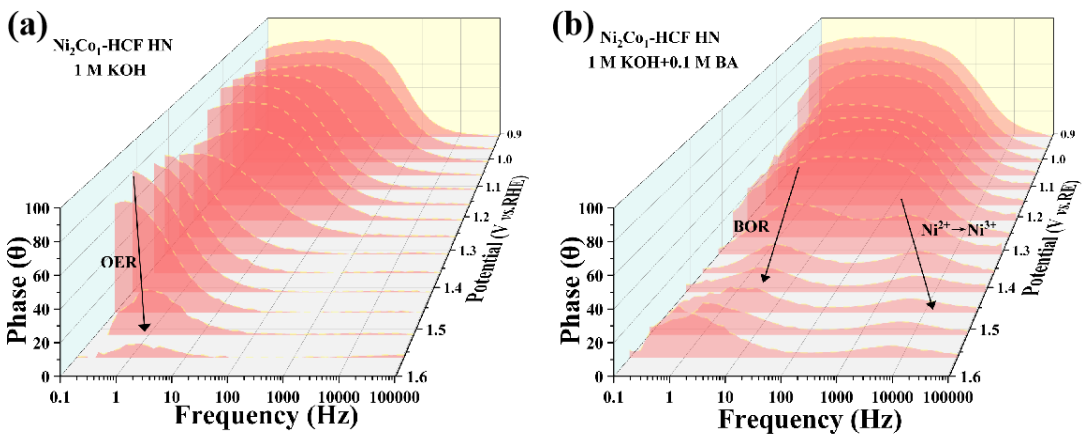

Fig. S9 Under different potentials using Operando EIS analysis of Ni_2Co_1-HCF HN in 1.0 M KOH (a) without and (b) with benzylamine.

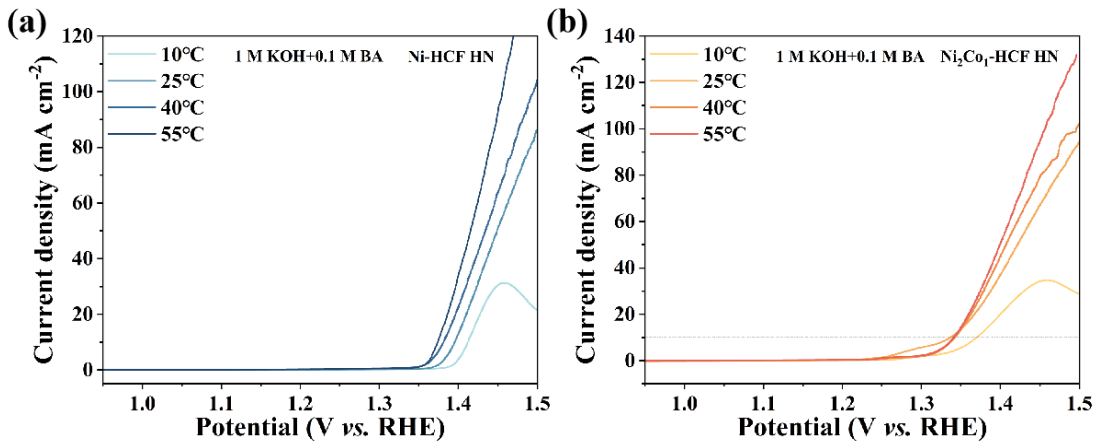

Fig. S10 The LSV curves of (a) Ni-HCF HN and (b) Ni_2Co_1-HCF HN in KOH solutions with 0.1 M benzyl alcohol as a function of temperature.

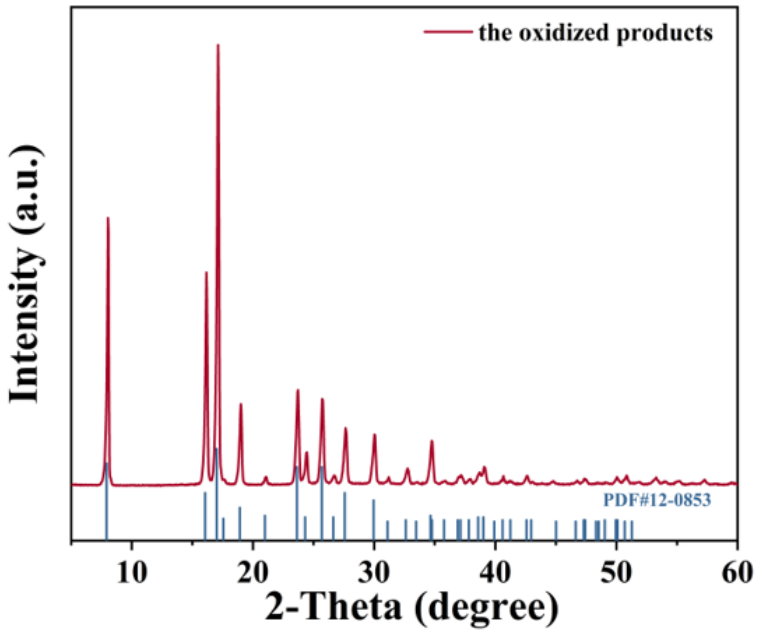

Fig. S11 The XRD pattern of the oxidized products.

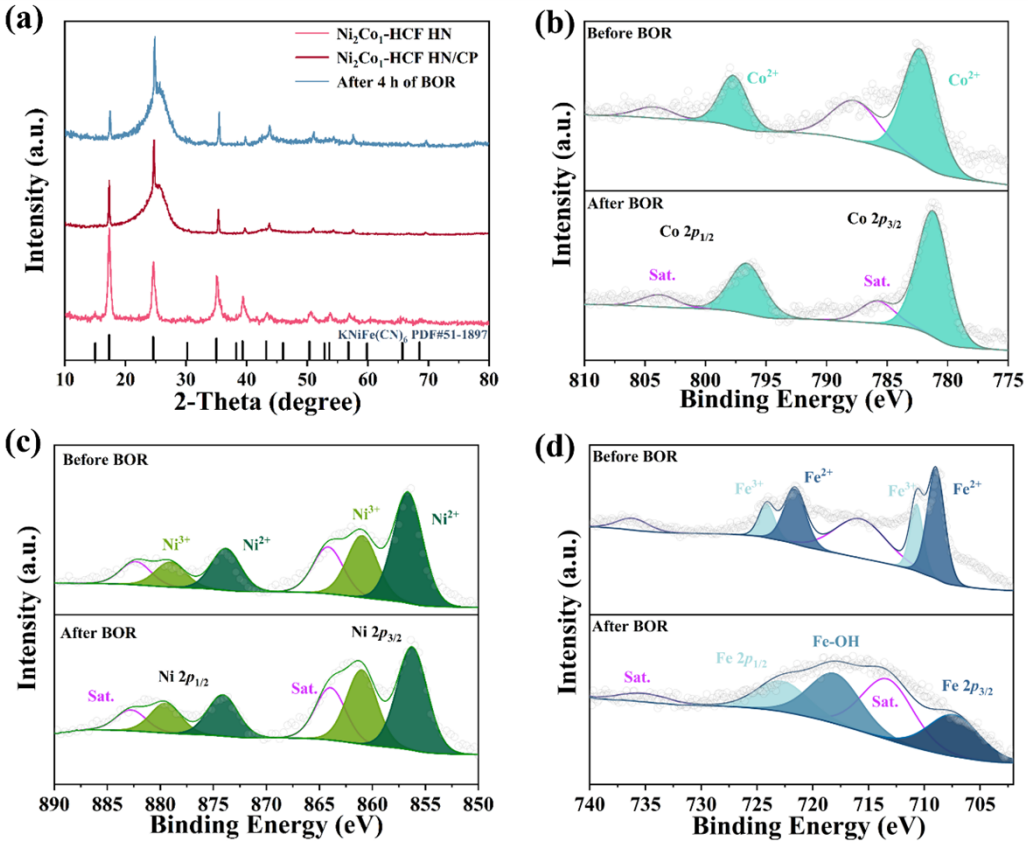

Fig. S12 (a) XRD spectra of Ni_2Co_1-HCF HN, Ni_2Co_1-HCF HN/CP and the samples after the reaction. High-resolution XPS of the sample before and after reaction. (b) Co 2*p*, (c) Ni 2*p*, and (d) Fe 2*p*.

Note 1

XRD results (Fig. S13a) reveal a negligible phase change for the sample deposited on carbon paper post 4 hours of BOR, this underscores the robust structural stability of the sample. The valence state changes on the surface of the sample before and after the reaction were tested by XPS. Fig. S13b shows the spectrum of Co, 782.1 eV and 796.8 eV can be attributed to $2p_{3/2}$/ and $2p_{1/2}$ of Co^{2+}. After BOR, there was no significant change in its valence state. Ni also has a similar trend (Fig. S13c). However, a noticeable valence state alteration in Fe was observed (Fig. S13d), resulting in the formation of significant Fe-O bonds. We believe this substantiates our claim that the creation of CN vacancies enhances the dangling bonds at Fe sites, thereby augmenting the potential for Fe-benzyl alcohol or Fe-oxygen species interactions.

Table S1 The elemental analysis data for Ni_2Co_1-HCF HN from ICP-OES results

Samples	Feed ratio of Ni:Co	Feed ratio of (NiCo):Fe	Content of Ni W (%)	Content of Co W (%)	Content of Fe W (%)	Measured ratio Ni:Co	Measured ratio (NiCo):Fe
Ni_2Co_1-HCF HN	**2:01**	**1:01**	**15.4**	**8.48**	**22.23**	**1.81:1**	**1.07:1**

Reference.

[S1] L. Yu, L. Zhang, H. B. Wu and X. W. (David) Lou, *Angew. Chem. Int. Ed.*, 2014, **53**, 3711–3714.